# AXIAL FORCE MODELLING AND MEASUREMENT IN A SINGLE STAGE CENTRIFUGAL PUMP

*Benoît Mary[1], Fabien Cerru[2]*

[1] Cetim, 74 route de la Jonelière, 44300 Nantes, benoit.mary@cetim.fr

[2] Cetim, 74 route de la Jonelière, 44300 Nantes, fabien.cerru@cetim.fr

## ABSTRACT

**Loads seen by a pump impeller over a wide range of operating flowrates are critical in designing its drive train. In the recirculation zones at lower flowrates (0.3Qn), loads can deviate significantly from empirical laws. To investigate these phenomena, a comparison between numerical simulations and experiments are carried out on a single volute horizontal Ns 70 (SI) pump.**

**The experimental tests are carried out using an array of strain gauges with on-board conditioners on a modified pump shaft. Torque, axial and radial forces are measured after static calibration.**

**The numerical simulations are performed using CFX with an unsteady RANS model, using the transient rotor-stator approach during a minimum of 8 revolutions. A Two-equation k-ε turbulence model combined to a 7 650 000 hexahedral elements model are used to compute the flow from 0.2 to 1.4Qn.**

**The measurements and the simulations exhibit a similar drop in traction forces around 0.3Qn, at the pre-rotation onset. A complete analysis of hydraulics instabilities leading to an inversion of the volute flow pattern explains the force drop.**

## KEYWORDS

PUMP MODELLING, LOADS, PRESSURE FLUCTUATIONS.

## NOMENCLATURE

| | |
|---|---|
| Ns | Specific speed (SI units) |
| RANS | Reynolds-Averaged Navier-Stokes |
| $D_{pipe}$ | Pipe diameter [m] |
| Q | Flow rate [kg/s] |
| Fa | Axial force on impeller [N] |
| CFD | Computational Fluid Dynamics |
| H | Head of the pump (m) |
| P | Power of the Pump (kW) |
| C | Torque of the pump (N.m) |
| D | Diameter of the impeller (m) |
| N | Rotational speed (rpm) |
| Φ | Diameter |
| Subscripts | |
| $X_n$ | BEP values of parameter X |
| Superscripts | |
| y+ | dimensionless meshing wall distance |

## INTRODUCTION

Radial thrust on impellers of centrifugal pumps has been investigated on a large range of pumps [1, 2, 3, 4, 5], both experimentally and numerically. Axial thrust has also been studied experimentally [6, 7], mainly close to the nominal operating point and for normal operating modes. To determine these forces, manufacturers use empirical methods, e.g. [8, 9, 10] to size the bearings and shaft. Other papers discuss the correlation between experimental measurements and numerical results [5, 11, 12, 13, 14, 15] for CFD validation purposes mainly but not to investigate axial thrust components at low flow rate. Away from the nominal flow rates, the flow through balancing holes and leakages through the gaps between the impeller and the casing, play an important part.

To compute the loads, the impeller is split in different parts, which see a specific pressure field obtained through the resolution of the modelled Navier-Stokes equations. The overall loads result from the pressure field integrated over the whole impeller surface.

To improve the understanding of hydraulic instabilities, experimental and numerical tests are carried out. A specific shaft with on-board strain gauges is developed and fitted on a single volute horizontal pump. Numerical simulations are performed with an unsteady model to quantify the load fluctuations. The experimental and numerical results are then compared. This study focuses on the axial forces at part load operations.

## EXPERIMENTAL SETUP

The tested pump is a single stage horizontal pump with a specific speed: $Ns = N\ Qn^{0.5}\ Hn^{-0,75}=70$. This pump has already been investigated numerically and experimentally under many conditions, including 4 quadrants (e.g. pump as turbine) [16, 17]. Its nominal performances are:

- Flow rate: 787.5 m3/h
- Head: 21 m
- Rotational speed: 1450 rpm

The main geometrical characteristics of the pump and impeller are presented in Table 1.

| Inlet parameters | Impeller | Outlet |
|---|---|---|
| Upstream duct Φ: 300 mm<br>Eye Φ: 224 mm<br>Hub Φ: 62.3 mm | Impeller Φ: 311.8 mm 6 blades (thickness: 4 mm, width b2 = 61 mm)<br>6 balancing holes: Φ=14 mm, length: 32 mm | Pump outlet Φ: 250mm<br>Volute cutwater Φ: 400 mm |

**Table 1: Pump geometrical parameters**

The clearance sizes are 0,25mm on the suction side and the balancing side.

The pump is installed on a closed test loop, allowing precise control of the inlet conditions (see Figure 1). The hydraulic parameters of the pump are measured according to the ISO 9906 standard for pump testing. The power of the pump is measured with a torque meter. An optical tachometer probe measures the rotation speed of the pump. An electromagnetic flowmeter is installed on the test loop. Differential pressure, upstream pressure, water temperature and vibrations are recorded. The pressure taps are located $2D_{pipe}$ upstream and $2D_{pipe}$ downstream of the pump flanges. The tests are performed at the nominal rotation speed of the pump (1450 rpm) and at 1050 and 725 rpm. All the load values obtained at a lower speed are then scaled to the nominal speed. The lower speed tests allow to explore a larger range of forces applied to the pump impeller to circumvent sensor range limitations and obtain information about the phenomenon at different speeds.

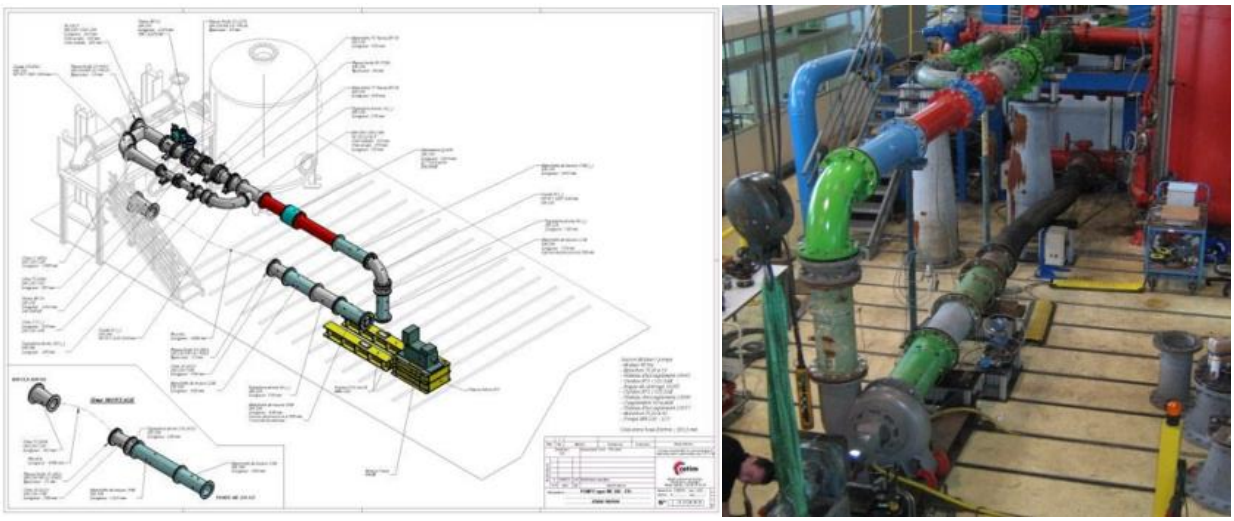

**Figure 1: Test rig diagram and picture**

The deformation of the shaft is monitored to compute the loads in different directions. To measure loads, the shaft has been modified. Its diameter is reduced to make room for strain gauges. The sensors are positioned between the impeller and the seal packing (see Figure 2). This reduction also increases the sensitivity of the sensors. The shaft is drilled to pass power and conditioning cables to the sensors. The conditioning units are attached to the pump coupling sleeve. The acceleration force seen by the different components (about 150 g) is within the equipment tolerance. Data are then transmitted wirelessly to record all the signals synchronously with a frequency of 4800 Hz.

Strain gauges are calibrated on a static bench and implemented to measure:

- Flexion at 0°; range: from -1500 to 1500 N;
- Flexion at 90°; range: from -1500 to 1500 N;
- Traction and compression; range: from -5000 to 5000 N;
- Torque; range: from -500 to 500 N.m.

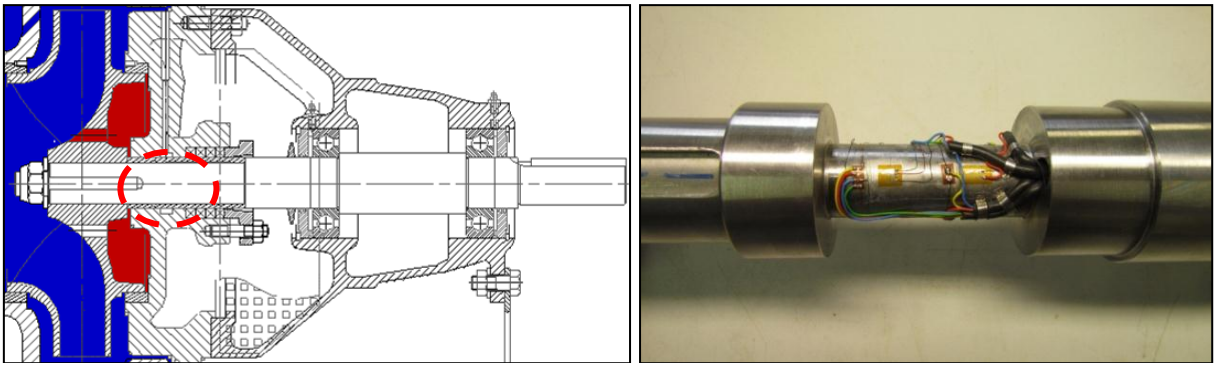

**Figure 2: Positioning of sensors on modified shaft**

## NUMERICAL STUDY

All computational simulations are carried out with ANSYS CFX v17.2. The computations run on workstations with the following technical characteristics: Bi-processors Intel Xeon @2.3GHz – 10 cores each, 64 Gb RAM. Validation of the CFD modelling of the pump against experimental data has been carried out in the past [3, 14, 16, 18].

### Geometry

The computational domain is broken down in three parts:

- the inlet duct including the inlet static part of the pump,
- the rotating domain including the impeller,
- the volute with the outlet pipe.

The pump geometry is obtained from the manufacturer's CAD files. Differences between the theoretical and the actual geometry, particularly near the leading edge of the blades, and on the leakage gaps between the impeller and the casing, can influence the numerical predictions. The actual leading edge of the blades are squarer than the model.

**Figure 3: Detail of the blade geometry – focus on the leading edge**

The position of the interfaces between the rotating part and stationary parts are presented on Figure 4. Each color represents one of the three parts of the computational domain. The inlet and outlet sections of the domain are positioned respectively at 5 $D_{pipe}$ upstream and 3 $D_{pipe}$ downstream.

The numerical model of the centrifugal pump includes:

- the volute,
- a six-blade open impeller with balancing holes,
- leakage gaps at the back and front of the impeller.

Sensitivity analyses have been performed to simplify the geometry and improve the computational time. However, the balancing holes and the leakage gaps are important in the computation of the loads and are considered in the current paper.

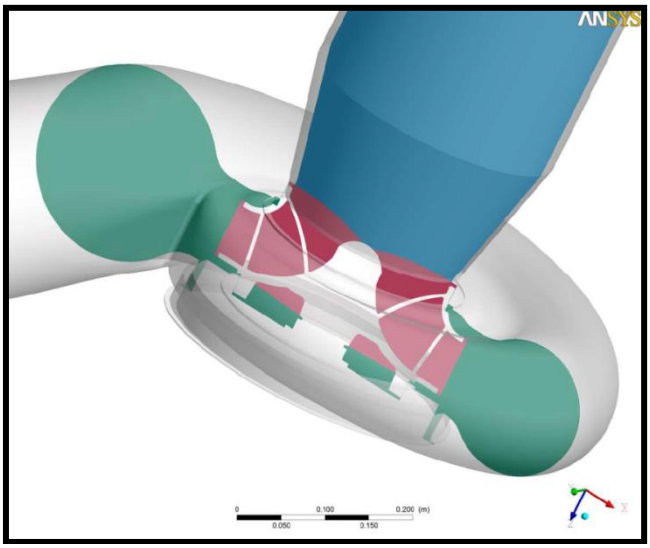

**Figure 4: Cross section of the computational domain**

**Mesh**

The mesh of the computational domain is constructed from a structured multi-block approach based on hexahedral elements. The grids are generated with ANSYS ICEM CFD software. The inlet duct, the impeller and the volute are fully meshed with no symmetry axis and no periodic assumption. The mesh sizes reach 485 000, 4 900 000 and 2 300 000 elements respectively. The structured grids are illustrated in Figure 5.

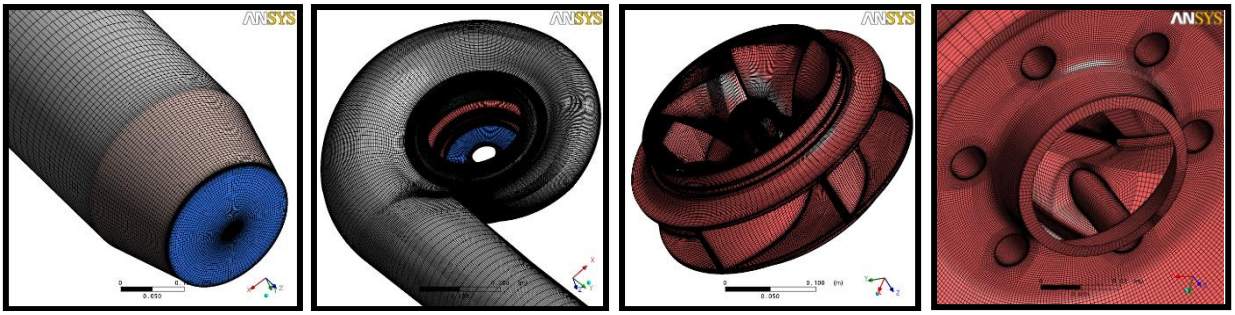

**Figure 5: Mesh visualizations of domains parts (inlet, volute and outlet pipe, impeller)**

Sensitivity analysis of the grid size has been performed to evaluate the influence of mesh density and mean values of y+ on the global values of the pump. The current mesh is the best trade-off between accuracy and computation time.

Mesh is refined near the walls to simulate wall velocity gradients with a law of the wall extrapolation. Specific cell thickness progression laws in the meridian, hub-to-shroud, and blade to blade directions are applied to ensure good grid quality: near wall orthogonality is enforced and the minimum angle observed in the domain corresponds to 23° (less than 1% of cells smaller than 30°).

The y+ average equals 50. Maximum value of y+ are around 200 and are located on the discharge side of the cutwater.

**Boundary conditions**

The fluid characteristics are set as ambient temperature water. A uniform mass flow rate is imposed at the inlet section and a relative pressure condition is used for the outlet condition for all operating point. These boundary conditions are similar to other references [3, 5, 12, 14, 16, 18].

**Modeling approach**

The turbulence is modelled with a two-equation approach based on the turbulent viscosity concept. The arguments related to the choice of the turbulence model (mainly SST or k-ε) are discussed in a previous article [3]. Based on these results, the k-ε model is used in the present study.

A transient Rotor-Stator approach is used to model interfaces between stationary and rotating parts (in red in Figure 4), where all quantities are transferred between stationary and rotating frames at each time step, allowing calculation of unsteady interaction phenomena. All computations are performed using a time step corresponding to an impeller angular increment of 2°. This value has been optimized, providing an acceptable compromise between computation time and output accuracy. The gap between the impeller and the volute is rather significant and as such does not require high-frequency time step. Several impeller rotations (up to eight rotations) may be necessary to correctly acquire instabilities such as “rotating stalls” which occur in certain operating conditions. Levels of RMS residuals of the time resolution are good for all the cases, reaching a value close to $10^{-6}$. The accuracy of the time and space discretization schemes is of the second order. The convective flows are computed using the Barth and Jespersen method, which is similar to a TVD_MUSCL scheme [19, 20, 21, 22].

A total of 18 computed operating points covering 0.15Qn - 1.4Qn are computed. A focus on off-design operating points, particularly in the pre-rotation region is carried out: 8 specific points from 0.15Qn to 0.5Qn are presented in this document.

## RESULTS PRESENTATION

**Transposition variables**

The measurements of the physical parameters have been performed at different rotation speeds (1450 rpm; 1050 rpm or 725 rpm). To compare the different results of the study with the computations

performed with a rotation speed of 1450 rpm, all the variables are scaled to the same speed using affinity laws:

$$\frac{Q_1}{Q_2} = \frac{N_1}{N_2}\left(\frac{D_1}{D_2}\right)^3 \qquad \frac{H_1}{H_2} = \left(\frac{N_1}{N_2}\right)^2\left(\frac{D_1}{D_2}\right)^3 \qquad \frac{C_1}{C_2} = \left(\frac{N_1}{N_2}\right)^2\left(\frac{D_1}{D_2}\right)^5$$

**Global performances**

The evolution of the head, efficiency and power as a function of the flowrate is plotted in Figure 6. The calculations are in good agreement with the experimental values. A slight overestimate of the head and an underestimate of the power lead to higher efficiencies. Mechanical losses are not considered in the calculations. It is to be noticed that the saddle type region (around 0.7Qn) is arguably well reproduced in the calculations. These simulations are detailed in reference [3].

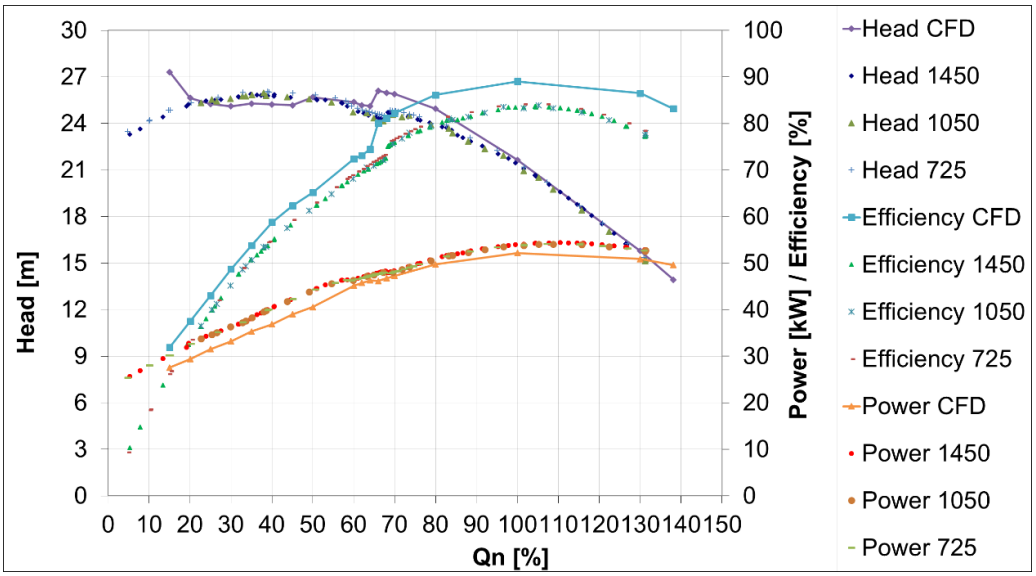


**Figure 6: Head, efficiency and power measured at 1450, 1050 and 725 rpm and scaled to 1450 rpm and CFD results**

**Flow description**

The flow patterns in the impeller are directly influenced by the flow rate. As noticed before, e.g. [4], for flow rates higher than 0.35Qn, a small recirculation zone occurs on the hub along the suction side of the blade. For lower flow rates, the recirculation zone moves towards the impeller inlet as described in [3]. The size of the recirculation zone increases as the flow rate decreases. This recirculation zone upstream of the inlet duct becomes more significant and grows upstream from a length of ½ $D_{pipe}$ at 0.5Qn to 4½ $D_{pipe}$ at 0.15Qn, as shown in Figure 7.

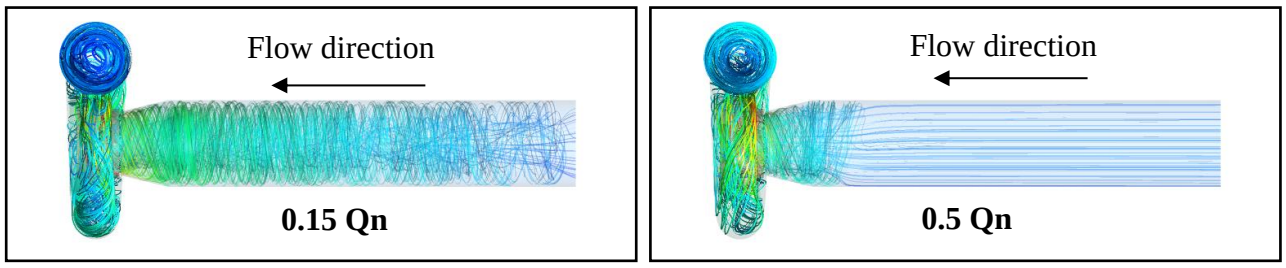


**Figure 7: Streamlines at the inlet duct**

**Local analysis and identification of hydrodynamic structures**

The local velocity field at flow rates around 0.3Qn shows an inversion of the flow rotation inside the volute compared to 0.2 or 0.4 Qn. This inversion carries on downstream of the pump. In Figure 8, the local velocity projected on the perpendicular plane and streamlines on outlet duct are presented fields for three flow rates with the same position of the impeller and after 8 full rotations.

The flow is driven between the blades, leaks to the inlet duct through the gap between shroud and volute (called “balancing gap”) and to the balancing zone through the gap between hub and volute (called “suction gap”). It finally returns to the main flow through the balancing holes.

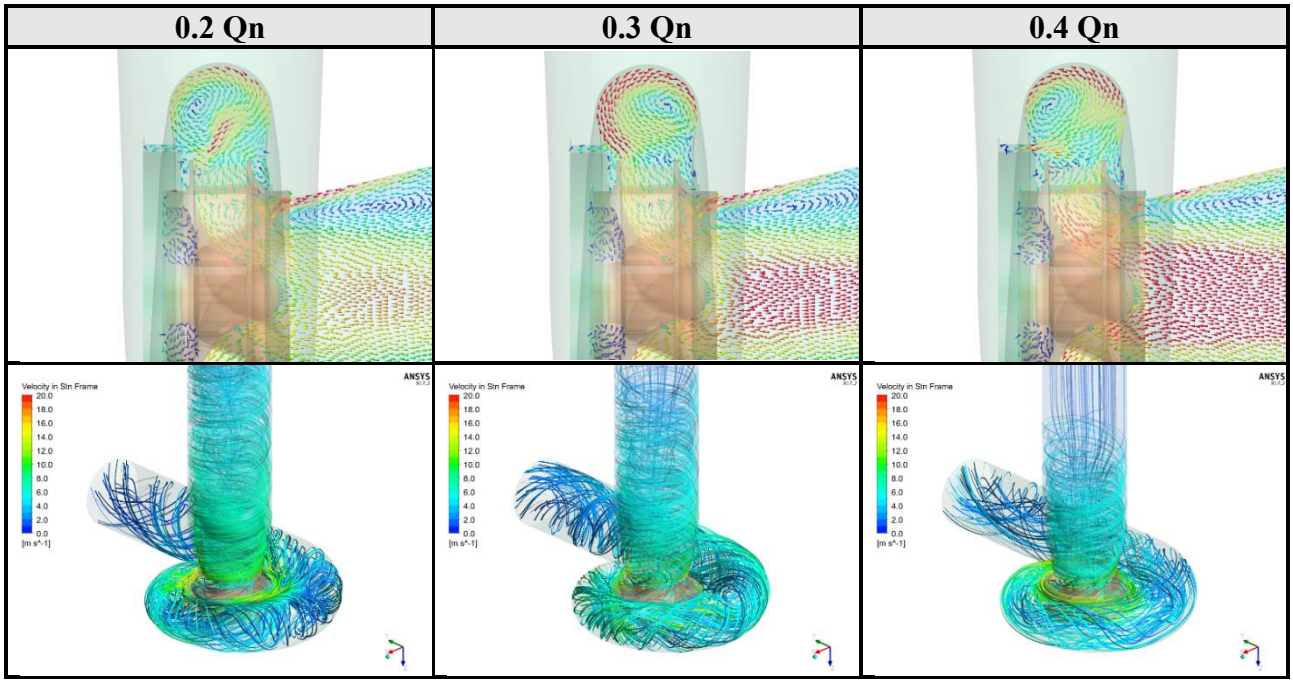


**Figure 8: Local instantaneous velocity field and streamlines in the volute**

The gap leak flowrates are significantly modified between 0.25 and 0.35Qn, as shown in Figure 9. Due to the inversion of the flow rotation, the leak through the balancing gap is increased, and the leak through the suction gap is reduced, leading to a drop in the overall axial forces acting on the impeller.

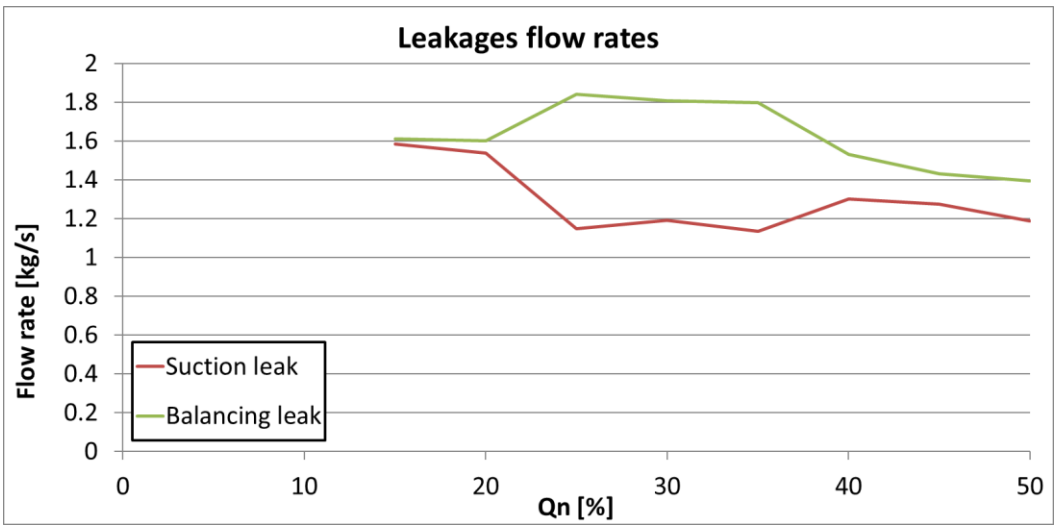


**Figure 9: Leakage flow rates at different flowrates**

**Axial thrust**

A significant drop of axial thrust occurs between 0.2 and 0.33Qn. Numerical simulations present a similar drop (see Figure 10), between 0.25 and 0.35Qn, with a small offset towards higher flowrates. However, the drop width and amplitude are correctly predicted.

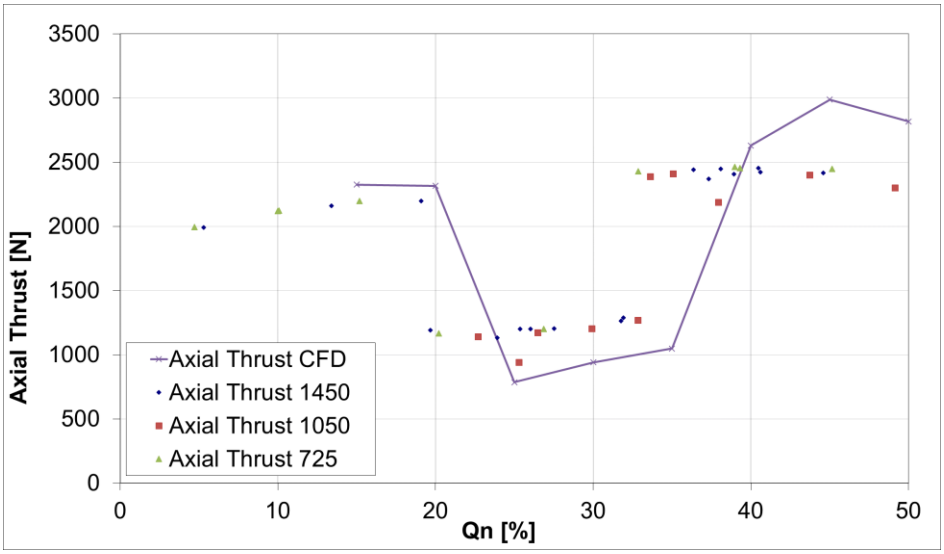


**Figure 10 Axial thrust – focus on pre-rotation drop (values scaled at 1450 rpm)**

A detailed analysis of the forces applying on the different parts of the impeller explains the contributing factors. Figure 12 shows the different contributions over the 0.15 to 0.5$Q_n$. The blades and the hub contribute to the same level of forces. The shroud has a negative impact. It can be noticed than the suction sides of the shroud and the hub are not impacted by the flow regime change around 0.3Qn. The increase in pre-rotation as the flowrate decreases does not affect the axial forces. The discharge sides of the hub and shroud exhibit the drop in axial force around 0.3 $Q_n$. The change of the recirculation pattern in the volute is responsible for this behavior. This specific flow could be due to the impeller and the casing design.

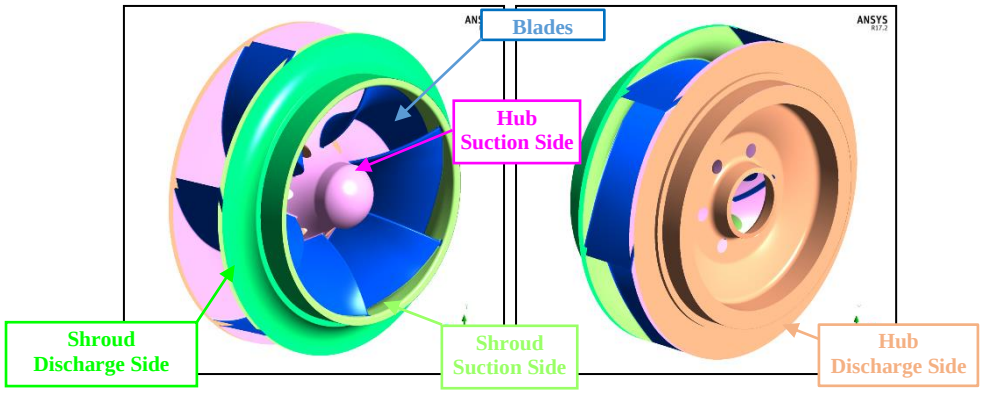


**Figure 11: Impeller zones**

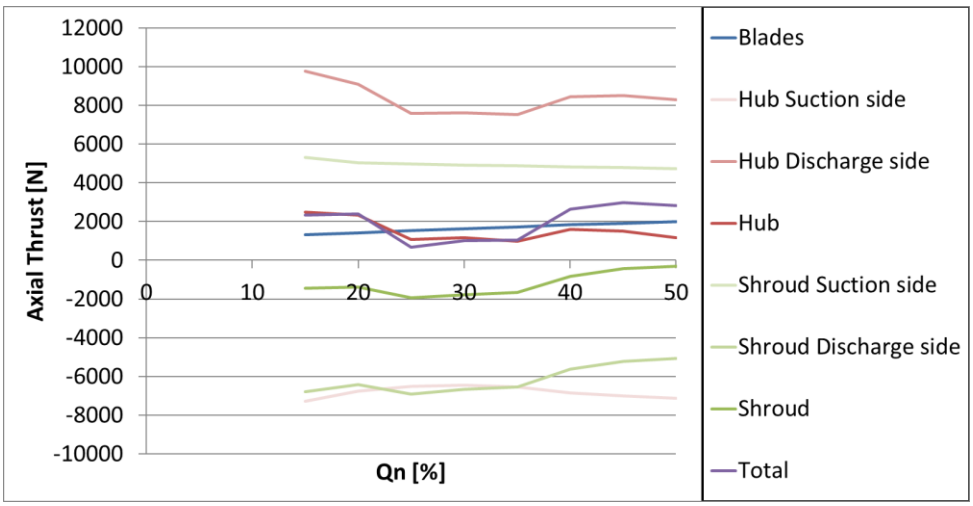


**Figure 12: Axial forces on impeller zones**

## CONCLUSIONS

The axial thrust in a centrifugal pump has been determined both experimentally and numerically on a wide range of flow conditions in a single stage centrifugal pump. The measures are carried out owing to the development of a specific instrumented shaft, which allows for real time / high frequency measurements of axial forces, radial forces, moments and their fluctuations.

The numerical study is performed in order to predict the drop of axial thrust in the pre-rotation region and explain the physical phenomena causing this instability. Full geometry simulations predict well the drop and the discontinuity of the traction curve. The decrease of axial thrust is due to the inversion of the flow's rotation, inducing variations of leakages flow rates as the flow rate is decreased from its nominal point. The next step is to carry out similar investigations on other pumps to validate or not the drop.

## ACKNOWLEDGEMENTS

The authors would like to thank the French pump manufacturers and the CETIM members of the working group on the operating conditions of centrifugal pumps in the 4-quadrants for their support.

## REFERENCES

[1] M. Asuaje, F. Bakir, S. Kouidri, F. Kenyery, and Robert Rey, (2005), Numerical Modelization of the Flow in Centrifugal Pump: Volute Influence in Velocity and Pressure Fields, International Journal of Rotating Machinery, vol. 2005, no.3, pp. 244-255

[2] J.F. Combes, A. Boyer, L. Gros, G. Pintrand, P. Chantrel, (2008), Experimental and numerical investigations of the radial thrust in a centrifugal pump, 12th ISROMAC, Honolulu, Hawai – USA

[3] A. Couzinet, L. Gros, and D. Pierrat, (2013), Characteristics of Centrifugal Pumps Working in Direct or Reverse Mode: Focus on the Unsteady Radial Thrust, International Journal of Rotating Machinery, vol. 2013, Article ID 279049

[4] K. Karaśkiewicz, & M. Szlaga (2014), Experimental and Numerical Investigation of Radial Forces Acting on Centrifugal Pump Impeller, Archive of Mechanical Engineering. 61, 10.2478

[5] Y. Nishi and J. Fukutomi, (2015), Component Analysis of Unsteady Hydrodynamic Force of Closed-Type Centrifugal Pump with Single Blades of Different Blade Outlet Angles, International Journal of Rotating Machinery, vol. 2015, Article ID 419736

[6] H. Abe, K. Matsumoto, J. Kurokawa, J. Matsui, Y-D Choi, (2008), Analysis and Control of Axial Thrust in Centrifugal Pump by Use of J-Groove, Transactions of the Japan Society of Mechanical Engineers Series B. 74. 10.1299/kikaib.74.317

[7] V. Godbole, R. Patil, S.S. Gavade, (2012), Axial Thrust in Centrifugal Pumps – Experimental Analysis, PAPER REF: 2977, ICEM15, Porto/Portugal

[8] J.F. Gülich (2010), *Centrifugal Pumps*, edition Springer

[9] Hydraulic Institute (2013), American National Standard for Rotordynamic Centrifugal Pumps for Design an Application, ANSI/HI 1.3-2013

[10] World Pumps, Experimental evaluation of axial thrust in pumps, (1999), Volume 1999, Issue 393, ISSN 0262-1762, https://doi.org/10.1016/S0262-1762(00)87551-3

[11] Z-H Han, P. Cizmas, (2001), A CFD Method for Axial Thrust Load Prediction of Centrifugal Compressors, International Journal of Turbo and Jet Engines, 20. 10.1115/2001-GT-0568

[12] Zhou, Ling & Shi, Weidong & Li, Wei & Agarwal, Ramesh, (2013), Numerical and Experimental Study of Axial Force and Hydraulic Performance in a Deep-Well Centrifugal Pump With Different Impeller Rear Shroud Radius, Journal of Fluids Engineering. 135, 104501, 10.1115/1.4024894

[13] Y. Bidaut, D. Dessibourg, The Challenge for the Accurate Determination of the Axial Rotor Thrust in Centrifugal Compressors, (2016), 2017-05-04T12:49:09Z; Asia Turb. & Pump Symposium

[14] A. Couzinet, L.Gros, D. Pierrat, L. Landry, (2011), 4-Quadrant Characteristics of Centrifugal Pump and Unsteady Computations of Abnormal Operating Points, Proc. 27th Inter. Pump Users Symposium, Houston, Texas

[15] B. Xia B, F. Kong, H. Zhang, L. Yang, & W. Qian, (2018), Investigation of axial thrust deviation between the theory and experiment for high-speed mine submersible pump, Advances in Mechanical Engineering

[16] L. Gros, A. Couzinet, D. Pierrat, L. Landry, (2011), Complete pump characteristics and 4-Quadrants diagram investigated by experimental and numerical approaches, AJK2011_06067, ASME Conference, Hamamatsu, Japan

[17] L. Gros, A. Couzinet, D. Pierrat, (2015), Part Load Flow and Hydrodynamic Instabilities of a Centrifugal Pump – PART 1: Experimental investigations, AJK2015_140444, ASME Joint Fluid Conference, Seoul, Korea

[18] L. Gros, A. Couzinet, D. Pierrat, (2015), Part Load Flow and Hydrodynamic Instabilities of a Centrifugal Pump – PART 2: Numerical simulations, AJK2015_140445, ASME Joint Fluid Conference, Seoul, Korea

[19] D. Pierrat, L. Gros, G. Pintrand, Modélisation des écoulements incompressibles, Approche couplée - découplée, les ouvrages du Cetim, ISBN : 978-2-85400-874-6

[20] F.R. Menter, (1993), Zonal Two Equation k-w Turbulence Models for Aerodynamic Flows, in 24th Fluid Dynamics Conference, AIAA Paper 93-2906, July, Orlando,

[21] F.R. Menter, (1996), A comparison of Some Recent Eddy- Viscosity Turbulence Models, Journal of Fluids Engineering, 118:514-519

[22] M.S. Darwish, F. Moukalled, (2003), TVD Schemes for unstructured grids, Int. Journal of heat and Mass Transfer, 46,4, 599-661